THE ASTROPHYSICAL JOURNAL, 449:145–155, 1995 August 10

PROBING THE GALACTIC DISK AND HALO. III. THE GALACTIC AND INTERGALACTIC SIGHT LINE TO H1821+643[1]

BLAIR D. SAVAGE,[2] KENNETH R. SEMBACH,[3,4] AND LIMIN LU[2,5]
Received 1994 October 31; accepted 1995 February 17

ABSTRACT

We present intermediate-resolution (FWHM $\sim$ 10–20 km s^{-1}) GHRS observations of interstellar and intergalactic absorption lines in the spectrum of the bright quasar H1821+643. The interstellar species detected include S II, Si II, Mg II, C IV, and N V. The intergalactic lines include Lyα (six lines), Lyβ (2 lines), Lyγ, and C III. The Galactic direction of H1821+643 ($l = 94\overset{\circ}{.}0$, $b = 27\overset{\circ}{.}4$) allows for the study of gas in the warped outer Galaxy since the effects of Galactic rotation cause absorption by distant gas to be Doppler-shifted by velocities approaching -190 km s^{-1}. We detect by Mg II and Si II extending from approximately $+40$ km s^{-1} to -150 km s^{-1}, indicating the presence of gas containing these metals in the outer Galaxy. Over the velocity range from -100 to -150 km s^{-1}, we find Si II/H I, Mg II/H I, and S II/H I $= 0.92 \pm 0.20$, ≥ 0.25, and ≤ 1.5 times the abundances of these elements in the Sun. However, the presence of C IV in this gas implies corrections must be made for the effects of ionization. A simple model allowing for the ionization by the EUV background suggests the measurements are consistent with absorption in a gas with an intrinsic metallicity of roughly 1/10 solar. Strong C IV and N V absorption is found in broad absorption centered near -8 km s^{-1}. This absorption is well represented with a component having a Doppler spread parameter, $b \sim 32$ km s^{-1}, N(C IV) $= (10.4 \pm 1.4) \times 10^{13}$ cm^{-2}, and N(N V) $= (14.3 \pm 2.6) \times 10^{13}$ cm^{-2}. The inferred column density ratio of C IV to N V of approximately 0.7 and the large line width suggests this gas is probably hot ($T > 2 \times 10^5$ K) and may be associated with Galactic radio loop III. The C IV doublet absorption also exhibits strong components centered near -70 and -120 km s^{-1}, which are not seen in N V. The -70 km s^{-1} C IV absorption probably is associated with highly ionized gas situated 1.5 kpc above the Perseus spiral arm. The -120 km s^{-1} absorption is likely associated with gas above the outer spiral arm of the Milky Way. Assuming corotation of disk and halo gas, a velocity of -120 km s^{-1} occurs at a Galactocentric distance of 24 kpc and a distance away of the plane of 7 kpc. The ionization of this distant gas may be produced by photoionization from the EUV extragalactic background radiation. We observe five intergalactic Lyα lines with W_λ(rest) > 60 mÅ over a redshift path of 0.057 implying a low-redshift Lyα cloud density in agreement with the local number density found toward 3C 273 by Morris et al. (1991). Combining the results for the two sight lines we obtain a Lyα cloud density $dN/dz = 73 \pm 19$ for $0 < z < 0.3$.

Subject headings: Galaxy: halo — ISM: abundances — quasars: absorption lines — quasars: individual (H1821+643) — ultraviolet: ISM

1. INTRODUCTION

The bright, low-redshift quasar H1821+643 ($V = 14.24$, $z = 0.297$) lies in the interesting Galactic direction $l = 94\overset{\circ}{.}0$ and $b = 27\overset{\circ}{.}4$ where the warp of the Milky Way extends to large Galactic latitudes and exhibits H I 21 cm emission with velocities as large as $v_{LSR} \sim -150$ km s^{-1} (Burton & te Lintel Hekkert 1985; Diplas & Savage 1991). Ultraviolet absorption-line measurements of H1821+643 provide an opportunity to study the distribution, composition, and physical conditions of gas in the outermost regions of the Milky Way and to study low-redshift intergalactic H I clouds. Low spectral resolution observations (FWHM $\sim$ 240 km s^{-1}) with the Faint Object Spectrograph (FOS) on the *Hubble Space Telescope* (*HST*) revealed extremely strong Galactic interstellar absorption toward H1821+643 (Savage et al. 1993a) and suggested that follow-up higher resolution observations would be important for a more detailed assessment of the absorption properties toward this quasar.

In this paper we present intermediate-resolution measurements (FWHM $\sim$ 10–20 km s^{-1}) of interstellar S II, Si II, Mg II, C IV, and N V absorption and intergalactic H I and metal-line absorption toward H1821+643 obtained with the Goddard High Resolution Spectrograph (GHRS). This work builds upon our earlier studies of neutral and highly ionized gas in the outer Galaxy along the NGC 3783 sight line (Lu, Savage, & Sembach 1994) and in the inner Galaxy toward HD 156359 (Sembach, Savage, & Lu 1995a). For a comprehensive discussion of the observations and theories of highly ionized gas in the Galactic halo, see Sembach & Savage (1992).

The GHRS observations of H1821+643 and data reductions are discussed in § 2. The Galactic sight line to H1821+643 is reviewed in § 3. We discuss the implications of measures of Si II, Mg II, and S II absorption at high negative velocity in § 4. The nature of the highly ionized Galactic gas toward H1821+643 is discussed in § 5. Results relevant to the

[1] Based on observations obtained with the Goddard High-Resolution Spectrograph on the NASA/ESA *Hubble Space Telescope*, obtained at the Space Telescope Science Institute, which is operated by the Association of Universities for Research in Astronomy, Inc., under NASA contract NAS 5-26555.

[2] Washburn Observatory, University of Wisconsin-Madison, 475 N. Charter Street, Madison, WI 53706; savage@madraf.astro.wisc.edu.

[3] Center for Space Research, 6-216, Massachusetts Institute of Technology, 77 Massachusetts Avenue, Cambridge, MA 02139; sembach@sundoggie.mit.edu.

[4] Hubble Fellow.

[5] Current address: Astronomy Department, 105-24, Caltech, Pasadena, CA 91125; ll@troyte.caltech.edu.

TABLE 1

GHRS OBSERVATIONS OF H1821+643

Observation[a] Identification	Grating	Wavelength Coverage (Å)	Resolution[b] (FWHM) (km s^{-1})	Date of Observation	Integration Time (minutes)	ISM Species Detected
Z15F0208M	G160M	1231.7–1268.9	20 + wings	1993 Apr 17	120[c]	N v, S ii, Si ii
Z15F020AM.....	G270M	2775.6–2822.7	10 + wings	1993 Apr 17	57	Mg ii
Z27N0108M.....	G160M	1231.7–1268.9	18	1994 Apr 5	171[c]	N v, S ii, Si ii,
Z27N010BN.....	G160M	1521.2–1557.5	14	1994 Apr 5	266	Si ii, C iv

[a] *HST* archive identification number. All observations were obtained with the light of H1821+643 in the Large Science Aperture. All exposures employed Digicon scanning step-pattern no. 4 (two substeps per diode and background samples obtained to each side of the object spectrum) and the FP-Split = 4 procedure to reduce detector fixed pattern noise.

[b] The pre-COSTAR spectra obtained before 1994 January have line spread functions with sharp cores and broad wings. In the post-COSTAR spectra the amount of energy in the wings is greatly reduced (see § 2).

[c] The 171 minute post-COSTAR spectrum is of substantially higher quality than the 120 minute pre-COSTAR spectrum both in terms of the higher S/N and the higher spectral resolution. Rather than combining the two spectra we have based most of our analysis on this post-COSTAR integration.

intergalactic medium at low redshift are given in § 6. A summary of this study is found in § 7.

2. OBSERVATIONS AND DATA REDUCTIONS

The GHRS measurements of H1821+643 listed in Table 1 were obtained on 1993 April 17 and 1994 April 5 as part of programs GTO-4094 and GO-5299. The characteristics of the GHRS are described by Soderblom et al. (1994) and Brandt et al. (1994). These intermediate-resolution integrations were obtained using the Large Science Aperture (LSA) and the G160M grating to cover the 1232–1269 Å and 1521–1558 Å regions and the G270M grating to cover the 2776–2823 Å region. The total integration times ranged from 57 to 266 minutes with ≈11% of these times spent measuring the detector background. The integrations were obtained with detector substep pattern 4, which provides two samplings per diode. The FP-split and four-diode comb-addition options were used to reduce fixed pattern noise from the detector window, photocathode, and diodes. The on-board Doppler compensation was enabled during the observations to correct for spacecraft motion. The centering of the object in the LSA was verified by LSA images obtained before each integration.

Our data involves pre-COSTAR and post-COSTAR spectra. COSTAR refers to the corrective optical system installed in the *HST* during the 1993 December Space Shuttle repair mission. The pre-COSTAR LSA spectra have line spread functions with sharp cores and broad wings. The cores have FWHM ~ 20 and 10 km s^{-1} at 1250 and 2800 Å, respectively. The wings caused by the aberrated *HST* image extend approximately ±70 and ±40 km s^{-1}, respectively, and contain ≈60% of the area of the line spread function. The line spread functions of the post-COSTAR spectra are adequately represented by Gaussian functions with FWHMs of 18 and 14 km s^{-1} at 1250 and 1550 Å, respectively. Rather than averaging the two spectra which have different resolutions, we emphasize the post-COSTAR spectrum in our analysis.

The data reduction techniques used here are identical to those discussed in Lu et al. (1994). We used the instrumental calibrations available in 1993 May for the pre-COSTAR data and 1994 May for the post-COSTAR data. The absolute wavelength calibration of our GHRS data is accurate to approximately one diode width, which corresponds to 17, 15, and 10 km s^{-1} at 1250, 1550, and 2800 Å, respectively. The good velocity correspondence between the saturated absorption of the Si ii λλ1260, 1526, and Mg ii λλ2796, 2803 lines, indicates that the relative velocity scales have an accuracy of ±5 km s^{-1}.

The spectra are plotted as count rate versus vacuum heliocentric wavelength in Figure 1. The interstellar absorption lines identified in Figure 1 are listed in Table 2. Additional absorption lines due to intergalactic absorption are listed in Table 3. To define local continua for the absorption lines identified in Figure 1, we fit low-order (<5) polynomials to regions free of absorption on either side of each line. Continuum normalized versions of the interstellar profiles are shown in Figure 2 as a function of LSR velocity ($v_{\rm LSR} = v_{\rm helio} + 13$ km s^{-1}). Equivalent widths, W_λ, ±1 σ errors, and integration limits for the interstellar lines detected with greater than 3 σ significance are listed in Table 2. The errors in W_λ reflect uncertainties due to both photon counting statistics and continuum placement errors (see Sembach & Savage 1992). Errors due to scattered light background uncertainty are small (<1% of the listed values of W_λ) as a result of the good scattering properties of the first-order GHRS gratings. A check on the validity of the total background correction comes from the cores of the strongly

TABLE 2

INTERSTELLAR ABSORPTION-LINE MEASUREMENTS

Ion	λ[a] (Å)	f[a]	v_-(LSR)[b] (km s^{-1})	v_+(LSR)[b] (km s^{-1})	$W_\lambda \pm 1\,\sigma$ (mÅ)
S ii	1250.584	0.00545	−150	+50	202 ± 26
S ii	1253.811	0.0109	−150	+50	264 ± 23
S ii	1259.519	0.0162	−150	+50	347 ± 22
Si ii	1260.422	1.007	−180[c]	+100[c]	868 ± 34
Si ii	1526.707	0.110	−200	+100	918 ± 20
Mg ii.....	2796.352	0.612	−200	+100	1890 ± 33
Mg ii.....	2803.351	0.306	−200	+100	1817 ± 40
N v	1238.821	0.157	−120	+100	189 ± 32
N v	1242.804	0.0782	−120	+100	122 ± 33
C iv	1548.195	0.191	−270	+100	624 ± 30
C iv	1550.774	0.0952	−270	+100	431 ± 32

[a] Wavelengths and *f*-values are from Morton 1991 except for Si ii λ1526 where we adopt the value recommended by Spitzer & Fitzpatrick 1993.

[b] Velocity integration limits for the equivalent widths.

[c] Si ii λ1260 integration limits are imposed by S ii λ1259 absorption at negative velocities ($v \le -180$ km s^{-1}) and an intergalactic medium line at positive velocities ($v \ge +100$ km s^{-1}).

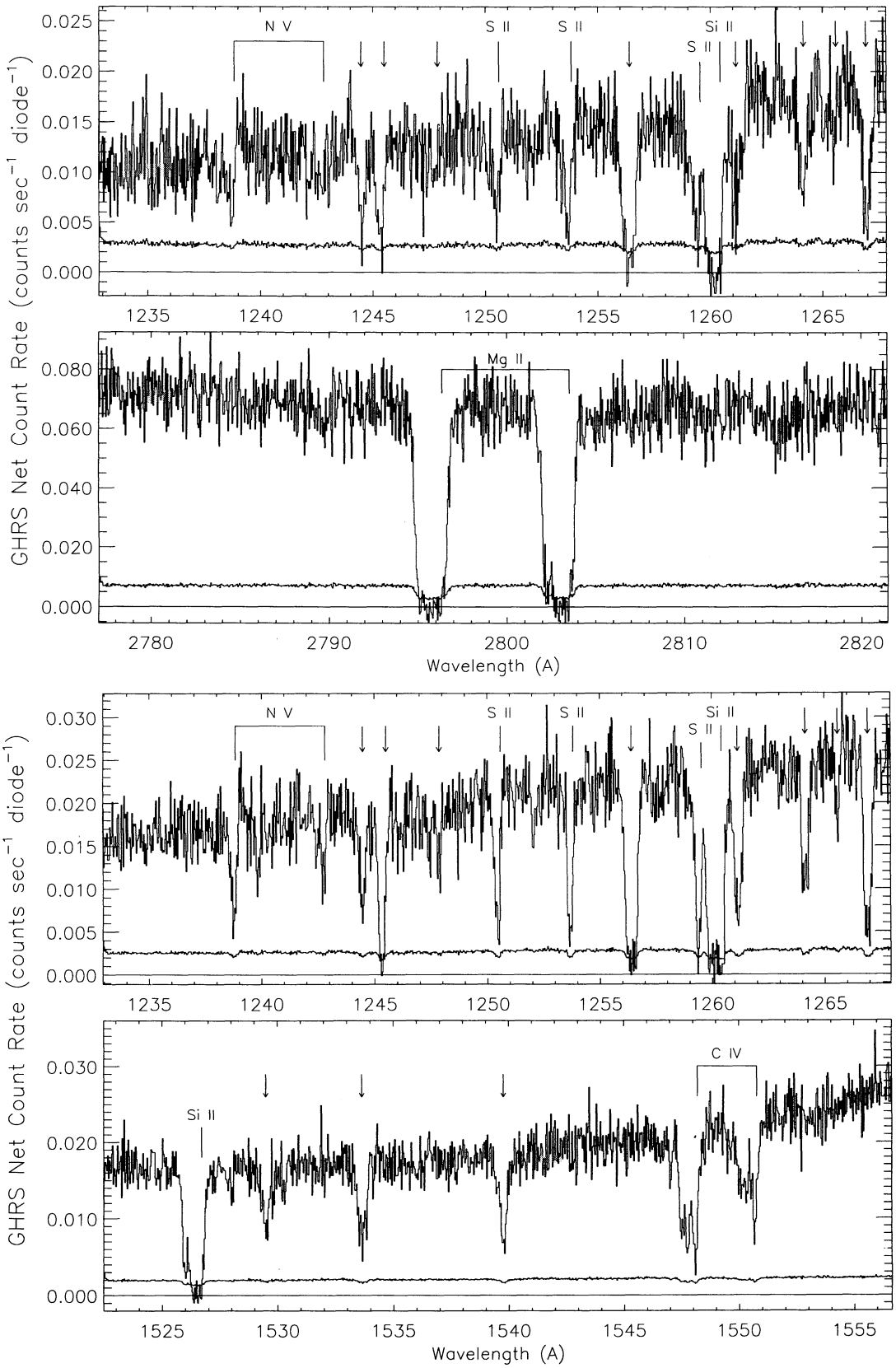

FIG. 1.—Count rate vs. heliocentric vacuum wavelength is plotted for the GHRS G270M and G160M spectra of H1821+643 listed in Table 1. The 1 σ error spectra are also shown. The two upper spectra were obtained before the installation of COSTAR. The two lower spectra were obtained after the installation of COSTAR. The resolution improvement associated with the corrective optics is clearly evident by comparing the pre- and post-COSTAR spectra of the 1233–1268 Å spectral region. The interstellar lines detected with greater than 3 σ significance (see Table 2) are identified on the spectra according to the ion type with the tick marks appearing at $v_{LSR} = 0$ km s^{-1}. The other lines detected with greater than 3 σ significance are noted on the spectra with arrows and identified in Table 3 as intergalactic lines.

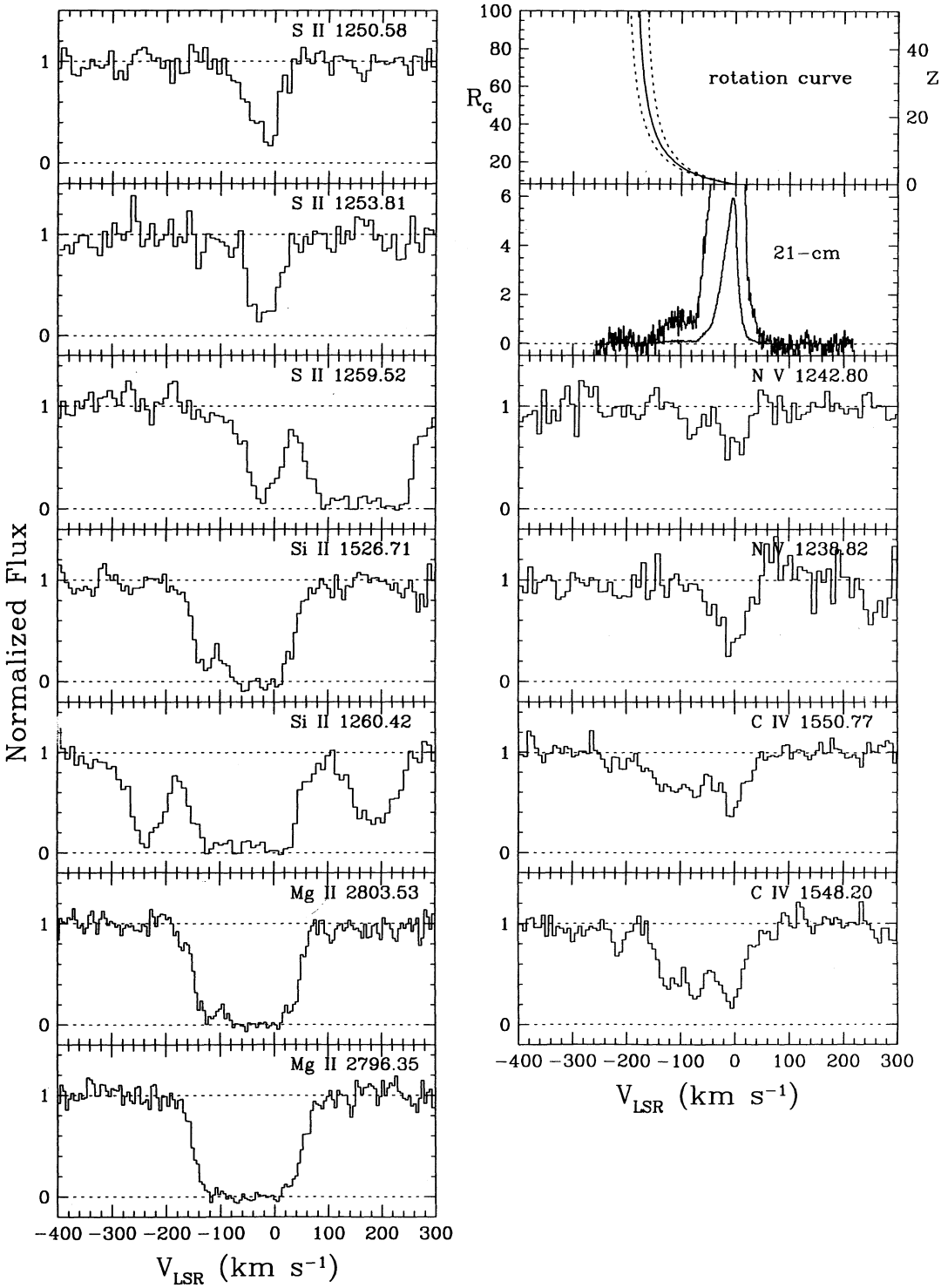

FIG. 2.—GHRS continuum normalized interstellar absorption line profiles for H1821+643 are plotted against LSR velocity. The absorption lines illustrated are listed in Table 2 and identified in Fig. 1. In several cases absorption by more than one species appears in the velocity region illustrated. These include: N V λ1238.82 with a marginally detected Mg II λ1239.93 absorption appearing at +267 km s^{-1}; Si II λ1260.42 with S II λ1259.52 appearing at $v_{LSR} = -215$ km s^{-1} and intergalactic Lyγ appearing near $v_{LSR} = +200$ km s^{-1}; and S II λ1259.52 with Si II λ1260.42 appearing at +215 km s^{-1}. At the top of the right panel we also show the LSR velocity to distance conversion assuming corotation of disk and halo gas and a flat Galactic rotation curve with $\Theta(R_G \geq 8.5 \text{ kpc}) = 220$ km s^{-1}. Scales for both Galactocentric distance, R_G (kpc), and distance away from the Galactic plane, z (kpc), are given. The dotted curves illustrate the effects of an error of ± 20 km s^{-1} error in the adopted value of $\Theta(R_G)$. We illustrate the Galactic H I 21 cm emission line observations for the direction to H1821+643 obtained with the NRAO 43 m telescope by Lockman & Savage (1995). Antenna temperature (K) is plotted against LSR velocity. The temperature scale is expanded by a factor of 10 for the upper display of the radio data.

TABLE 3

SINGLE-COMPONENT FITS TO THE INTERGALACTIC LINES

Wavelength[a] (Å)	$W_\lambda \pm 1\ \sigma$[b] (mÅ)	ID	$z \pm 1\ \sigma$	$b \pm 1\ \sigma$ (km s^{-1})	$N \pm 1\ \sigma$ (cm^{-2})
1244.466.....	184 ± 23	Lyβ	0.21326 ± 0.00003	38.9 ± 5.5	2.87 ± 0.57 (14)
1245.500.....	297 ± 23	Lyα	0.02454 ± 0.00001	30.8 ± 2.5	1.40 ± 0.27 (14)
1247.858.....	52 ± 16	Lyβ	0.21656 ± 0.00004	25.0 ± 7.6	9.66 ± 3.99 (13)
1256.400.....	459 ± 27	Lyβ	0.22489 ± 0.00001	50.9 ± 2.9	2.28 ± 0.40 (15)
1261.124.....	227 ± 16	Lyγ	0.29674 ± 0.00002	58.1 ± 4.2	1.65 ± 0.17 (15)
1264.138.....	206 ± 18	Lyα	0.03987 ± 0.00002	47.0 ± 4.0	5.59 ± 0.68 (13)
1265.579.....	47 ± 14	Lyα	0.04105 ± 0.00002	16.4 ± 5.4	1.08 ± 0.49 (13)
1266.917.....	247 ± 19	C III	0.29672 ± 0.00001	41.8 ± 2.5	7.68 ± 0.77 (13)
1529.486.....	168 ± 21	Lyα	0.25814 ± 0.00003	47.6 ± 5.3	3.99 ± 0.60 (13)
1533.635.....	206 ± 17	Lyα	0.26156 ± 0.00002	44.0 ± 3.7	5.82 ± 0.68 (13)
1539.773.....	206 ± 22	Lyα	0.26660 ± 0.00002	37.9 ± 3.0	4.98 ± 0.56 (13)

[a] Vacuum heliocentric wavelength.
[b] Equivalent widths and their errors are listed in the rest frame.

saturated interstellar lines of Mg II λλ2797, 2803 and Si II λλ1260, 1526 in the velocity range from −50 to +20 km s^{-1} where the H I column density is large (21 cm H I antenna temperature >0.5 K; see Fig. 2). We note an elevation in flux from −20 to −60 km s^{-1} in the core of the Si II λ1260 line, which amounts to ∼7% of the continuum flux. Careful examination of the reduction processes indicates that the excess flux is probably due to noise.

To describe the complex high-ionization absorption, we employ the profile fitting method (Sembach, Danks, & Savage 1993) and find that the C IV and N V absorption is well described by the multicomponent fit results listed in Table 4. The indicated values of C IV component velocity, $\langle v_{LSR} \rangle$, Doppler spread parameter, b, and column density, N, were obtained by fitting the stronger λ1548 line. These results are consistent with the λ1550 profile. A comparison of the weak and strong line apparent optical depth profiles (Savage & Sembach 1991) shows that C IV lines are not saturated. Therefore, the total column density estimate is reliable even though the true absorption structure may be more complex than the simple four-component model adopted. The N V fit result for component 1 is based on a fit to the broad λ1238 profile. The N V 3 σ upper limits for components 2, 3, and 4 were obtained by integrating the error spectrum for the N V λ1238 line over a velocity range defined by 2 × FWHM = 3.332 × b(C IV), where b(C IV) is the Doppler spread parameter for the corresponding C IV component. We consider the feature of low statistical significance in the N V λ1242 profile at ≈ −80 km s^{-1} to be either noise or a contaminating intergalactic Lyα line, since it does not appear in the stronger N V λ1238 profile.

TABLE 4

INTERSTELLAR COMPONENTS OF C IV AND N V[a]

Ion	Component	$\langle v_{LSR} \rangle$ (km s^{-1})	b (km s^{-1})	N (cm^{-2})
C IV.....	1	−8.2 ± 3.7	29.4 ± 3.3	10.4 ± 1.4 (13)
	2	−70.0 ± 3.9	18.0 ± 4.1	6.0 ± 1.6 (13)
	3	−120.3 ± 5.4	24.8 ± 3.1	6.1 ± 1.1 (13)
	4	−213.3 ± 3.0	11.6 ± 2.7	1.2 ± 0.3 (13)
N V.....	1	−6.9 ± 5.7	34.8 ± 4.4	14.3 ± 2.6 (13)
	2	−70.0	...	<3.5 (13)[b]
	3	−120.3	...	<4.2 (13)[b]
	4	−213.3	...	<2.7 (13)[b]

[a] The component fits based on the N V λ1238 and C IV λ1548 line profiles shown in Fig. 2.
[b] Upper limits on components 2–4 for N V are 3 σ limits derived by integration of the error spectrum for the velocity range defined by 2 × FWHM = 3.332b(C IV).

In Table 3 we list the observed wavelengths, identifications, and rest frame equivalent widths of the intergalactic lines with greater than 3 σ significance. We performed single Gaussian component fits to each of the intergalactic medium (IGM) lines to determine the values of redshift, z, Doppler spread parameter, and column density listed in Table 3. For all intergalactic lines, the profile fits were performed over a ±400 km s^{-1} velocity range. The IGM lines are weak enough that contributions to the absorption by radiation damping wings are unimportant.

The H I 21 cm emission line spectrum for the H1821+643 direction is shown near the top of the right panel of Figure 2. These H I data were obtained with the NRAO 43 m radio telescope (21′ FWHM beam) and have been corrected for radio antenna side lobe contamination. The H I emission extends from v_{LSR} = +46 to −146 km s^{-1}, peaks near −4 km s^{-1}, and has an average velocity of −15 km s^{-1} (Lockman & Savage 1995). The total H I column density is 3.81 × 10^{20} cm^2 assuming the emission is optically thin. The H I emission from about −100 to −145 km s^{-1} in this direction is likely associated with the warp of the distant Galaxy, which can be traced in the second Galactic quadrant to latitudes as large as 25°–30° (Burton 1988; Diplas & Savage 1991).

3. THE GALACTIC SIGHT LINE TO H1821+643

Absorption along extended sight lines through the Milky Way is usually influenced by a variety of Galactic phenomena, and the H1821+643 sight line (l = 94°.0, b = +27°.4) is no exception to this rule. The sight line passes through the local hot bubble, close to a nearby planetary nebula (K1-16), near the boundary of Galactic radio loop III, over the Perseus and outer spiral arms, and through the outer Galactic warp.

Absorption velocities along the H1821+643 sight lines are strongly influenced by differential Galactic rotation. In Figure 2, we illustrate the relationship between LSR velocity and Galactocentric distance, R_G, for the H1821+643 direction assuming a flat rotation curve with $\Theta(R_G \geq 8.5\ \mathrm{kpc}) = \Theta_\odot$ = 220 km s^{-1} and $R_\odot$ = 8.5 kpc. The dotted curves bracket the range of expected velocities due to a ±20 km s^{-1} error in $\Theta_\odot$. The distance of the sight line from the Galactic plane, z, is shown at the right of the plot. In this direction the limiting LSR velocity for the assumed rotation curve is −190 km s^{-1}.

The outer "local bubble" boundary in the general direction of H1821+643 probably occurs within 100 pc of the Sun

(Vallerga et al. 1993). Models of the conductive boundary between the local bubble and the low-density neutral medium in which the Sun is embedded predict C IV columns ([0.9–2.7] $\times 10^{12}$ cm^2; Slavin 1989) that are $\sim$100 times less than those observed toward H1821+643. Observations of C IV toward stars within a few hundred pc of the Sun confirm that the nearby high ion absorption is weak (Edgar & Savage 1992).

H1821+643 lies several degrees inside the boundary of radio loop III, which is centered on $l = 124 \pm 2°$, $b = 15 \pm 3°$ and has a diameter of $65 \pm 3°$ (Berkhuijsen, Haslam, & Salter 1971). Loop III is located at an approximate distance of 150 ± 50 pc (Spoelstra 1972) and affects the local distribution of neutral material (see Heiles 1984). Since large amounts of highly ionized gas are known to exist along the 3C 273 sight line through radio loops I and IV (Burks et al. 1991; Savage et al. 1993b), it is also possible that loop III may contribute significantly to the observed high ion column densities toward H1821+643.

The H1821+643 sight line passes 96″ away from the central star of planetary nebula K1-16, which has an optical radius of 57″ (Kohoutek 1963; Acker et al. 1992). The nebula is evident in the CCD image of the field surrounding H1821+643 published by Kirhakos et al. (1994). The central star of K1-16 is a hot white dwarf with $T_{\rm eff} \approx 80{,}000$ K and a distance of about 1.6 kpc (Grauer & Bond 1984). The 57″ optical radius of K1-16 corresponds to 27 pc at the estimated distance. Models of the ionized regions around hot white dwarfs (Dupree & Raymond 1983) show that the optical radii of the nebulae should be much larger than the radius of the photoionized C IV and N V zones. Thus, we do not expect K1-16 to contribute to the C IV and N V absorption toward H1821+643.

The sight line to H1821+643 passes over a number of the spiral arms identified in H I emission (Kepner 1970) including the intermediate arm (-42 km s^{-1}), the Perseus arm (-75 km s^{-1}), and the outer arm (-93, -115 km s^{-1}). Here the numbers in parentheses indicate the approximate LSR velocities of the arms at low latitudes. The two velocities for the outer arm are for its inner (O_i) and outer (O_o) branches. The outer branch of the outer arm blends with another feature referred to as O* by Kepner. These outer spiral arm structures are part of the warped outer Milky Way.

The H1821+643 sight line also lies near the edge of high-velocity cloud complex C, whose nature and distance are uncertain. A general review of the properties of complex C is found in Wakker & van Woerden (1991). The H1821+643 sight line lies $\sim$3° outside the lowest ($T = 0.04$ K) H I boundary of complex C as delineated in the Wakker & van Woerden (1991) map. The nature of the intermediate and high-velocity sky is complex in this general direction of the Galaxy with overlapping spurs, arches, complexes, etc. (see Fig. 1 in Kuntz & Danly 1992). Verschuur (1993) has modeled the high- and intermediate-velocity H I distribution in the general direction of the Perseus spiral arm. In his model, complex C is part of an expanding supershell whose expansion is impeded by loop III. The expansion velocities expected in the model in the direction of H1821+643 are very large (≈ -180 km s^{-1}; see Verschuur's Table 2). However, complex C may be more distant than Verschuur's model assumes. Danly (1989) and deBoer et al. (1994) constrain the gas in complex C to be more than 1.5 kpc away from the Galactic plane in several directions. Haud (1988) has proposed that complex C is the counter part of the Magellanic Stream in the northern hemisphere and that both objects together form a polar ring around the Galaxy.

The total H I column density for Galactic gas toward H1821+643 of 3.81×10^{20} cm^2 from the 21 cm data of Figure 2 implies a total dust color excess $E(B-V) = 0.07$ assuming the H I to dust ratio, $\langle N({\rm H\ I})/E(B-V)\rangle = 5.27 \times 10^{21}$ cm^{-2} mag^{-1} recommended by Lockman & Savage (1995). Most of this dust is expected to be associated with the gas producing the strong H I 21 cm emission extending from $v_{\rm LSR} = \sim +30$ to ~ -60 km s^{-1} (see Fig. 2).

4. NEUTRAL AND WEAKLY IONIZED GALACTIC GAS

The interstellar absorption profiles shown in Figure 2 reveal strong absorption by Mg II $\lambda\lambda$2796, 2803, Si II $\lambda\lambda$1260, 1526, and S II $\lambda\lambda$1250, 1253, 1259. In the lines of Mg II and Si II strong absorption extends from $+40$ to -150 km s^{-1}, while for S II the absorption is strong from $+20$ to -80 km s^{-1}. We concentrate our attention on the absorption at large negative velocity between -100 and -150 km s^{-1} since that gas may be located at large Galactocentric distances (see the rotation curve in Fig. 2).

To account for the differing instrumental spread functions, line shapes, and line strengths in determining the implications of the Mg II, Si II, and S II absorption at these velocities, we compare the observed absorption profiles to those predicted from the observed H I 21 cm emission profile from Lockman & Savage (1995) shown in Figure 2. In the optically thin limit, the observed antenna temperature and column density per unit velocity are related through $N_{\rm H\,I}(v) = 1.82 \times 10^{18} T_a(v)$ (atoms cm^{-2}). Assuming the gas to be optically thin is reasonable since $T_a(v) < 0.15$ K and $\log N({\rm H\ I}) = \log \int N_{\rm H\,I}(v)dv = 18.79$ over the velocity range from -100 to -150 km s^{-1}. The H I column density and the predicted column density of the ion of interest are related at a given velocity through $N_x(v) = N_{\rm H\,I}(v)\delta_x(X/{\rm H})_\odot$, where $\delta_x = (X\ {\rm II}/{\rm H\ I})/(X/{\rm H})_\odot$ is the gas-phase abundance of element X in ion state II measured with respect to the solar abundance, $(X/{\rm H})_\odot$. We use the Anders & Grevesse (1989) solar abundances, $(X/{\rm H})_\odot = 3.89 \times 10^{-5}$, 3.55×10^{-5}, and 1.86×10^{-5}, for Mg, Si, and S, respectively, and make the simplifying assumption that δ_x is constant between -100 and -150 km s^{-1}.

A normalized intensity profile for the predicted column density profile of species X is given by $I_{px}(v) = e^{-\tau_x(v)} \otimes \phi(v)$, where $\tau_x(v) = N_x(v) f\lambda\pi e^2/m_e c$ is the predicted optical depth profile and $\otimes$ denotes a convolution with the instrumental spread function, $\phi(v)$. Here f and λ are the oscillator strength and wavelength of the transition and e, m_e, and c are the usual atomic constants.

To find the best values of δ_x over the -100 to -150 km s^{-1} velocity range, we minimize the differences between the predicted $I_{px}(v)$ and the observed intensity profile $I_{ox}(v)$ normalized by the continuum derived in § 2. The results of this exercise are shown in Figure 3 where we plot the observed profiles, $I_{ox}(v)$, for each of the three ions as filled circles along with the best-fit profile (or 2 σ limit profile for S II) with the solid line. $I_{px}(v)$ profiles for various other values of δ_x are shown with the dashed lines. We find $\delta_{\rm Mg} \geq 0.25$, $\delta_{\rm Si} = 0.92 \pm 0.20$, and $\delta_{\rm S} \leq 1.5$.

An estimate of the column densities of Mg II, Si II, and S II found by simply integrating the observed column density profiles,

$$N_x = \int N_x(v)dv = \int m_e c/f\lambda\pi e^2 \ln[1/I_{ox}(v)]dv\ ,$$

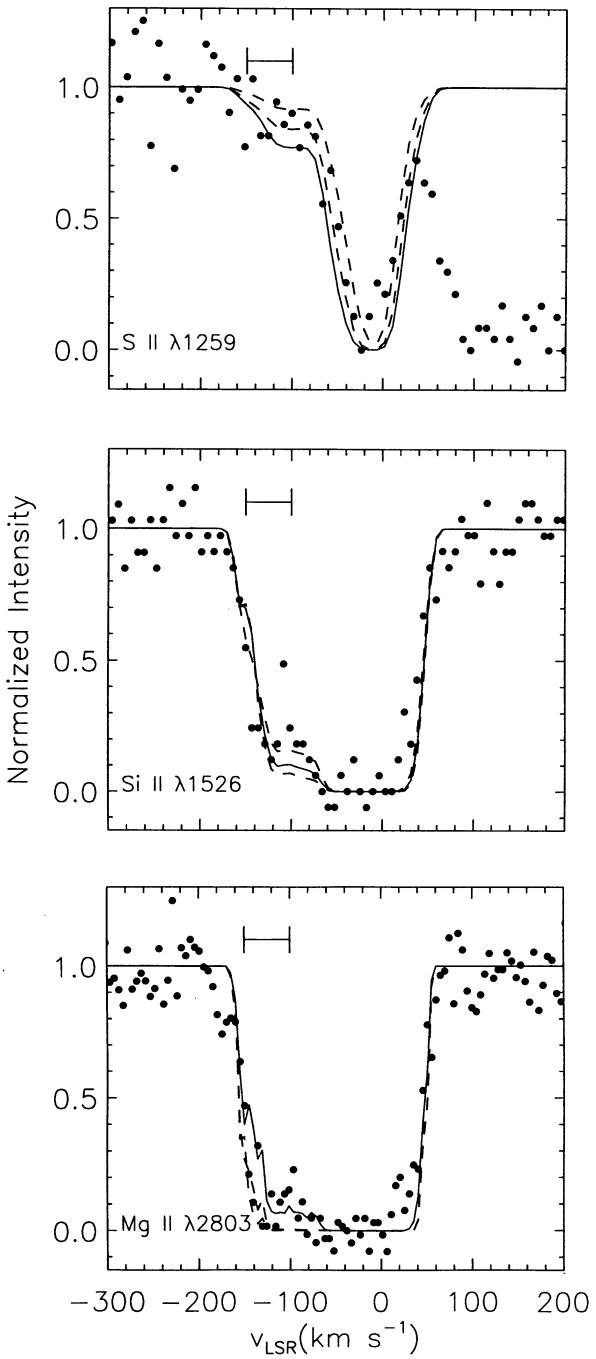

FIG. 3.—Model profile reconstruction results for the S II λ1259, Si II λ1526, and Mg II λ2803 lines as discussed in § 4. The filled circles indicate the measured data values in each case. The solid line indicates the profile for the best estimate or limit for $\delta_x = (X\ \text{II}/\text{H I})/(X/\text{H})_\odot$ for the three ions: $\delta_{Mg} \geq 0.25$, $\delta_{Si} = 0.92 \pm 0.20$, and $\delta_S \leq 1.5$. For S II and Mg II, the dashed curves indicate values of $\delta_x = 1.0$ and 0.5. For Si II the dashed curves indicate values of δ_{Si} that are 0.2 dex larger and smaller than the best estimate of 0.92. The −150 to −100 km s^{-1} range of interest for these estimates is indicated at the top of each panel.

between −100 and −150 km s^{-1} yields log N(Mg II) > 13.74, log N(Si II) > 14.24, and log N(S II) ≤ 14.04. With log N(H I) = 18.79 from the 21 cm data, these column densities imply $\delta_{Mg} > 0.23$, $\delta_{Si} > 0.79$, and $\delta_S \leq 0.95$. In this case, the lower limits on N(Mg II) and N(Si II) arise from underestimates in N(Mg II) and N(Si II) due to unresolved saturated structure at these velocities, inferred from comparisons with the $N_x(v)$ profiles for the stronger observed lines of Mg II and Si II. For Mg II this estimate does not include a correction for instrumental blurring of strong lower velocity absorption into the −100 to −150 km s^{-1} velocity range due to the broad wings on the aberrated *HST* spectral spread function. For S II and Si II this should not be a problem since the data were obtained after corrective optics were placed in front of the GHRS. Although these estimates are not as rigorous as those presented above, they provide a simple check on our calculations and are consistent with the more detailed treatment accounting for the velocity dependence and instrumental spread function effects.

Absorption at velocities between −100 and −150 km s^{-1} occurs in gas at R_G = 20–45 kpc (z = 8–20 kpc) assuming that the gas participates in Galactic rotation and that the rotation curve is flat with Θ = 220 km s^{-1} beyond the solar circle at $R_\odot$ = 8.5 kpc. Finding nearly solar metal abundances in this gas is surprising since many elements seem to exhibit a Galactocentric abundance gradient of approximately −0.08 dex kpc^{-1} (Shaver et al. 1983). Thus, we might expect gas at such large Galactocentric distances to be down in abundance by perhaps 1 dex compared to the solar values. Indeed, Lu et al. (1994) found gas in intermediate and high-velocity clouds toward NGC 3783 with S/H = 0.5 ± 0.2 solar (at v_{LSR} = +62 km s^{-1}) and S/H = 0.15 ± 0.05 solar (at v_{LSR} = +240 km s^{-1}). The observed abundance in the intermediate-velocity cloud was found to be consistent with that expected from the known metallicity gradient in the Galactic disk if the intermediate-velocity gas is a corotating high-z extension of an outer spiral arm at a Galactocentric distance of 14 kpc. The values of S/H in the HVC of 0.15 ± 0.05 favored the Magellanic Stream or an independent extragalactic object in the Local Group of galaxies interacting with the Galaxy as the likely origin of the HVC.

A plausible explanation for derived ionic ratios is that we are seeing the effects of photoionization in the low-density gas of the outer Galaxy which has intrinsic abundances much less than solar. C IV absorption is also seen in gas likely associated with the outer Galaxy in a component centered at −120 km s^{-1} (see § 5.3). We believe the origin of the C IV at such large Galactocentric distances is photoionization from the EUV extragalactic background radiation. The simple photoionization model discussed in § 5.3 reveals that values of the ionization parameter log Γ = −3.1 in a gas with 1/10 solar abundances can produce a C IV column density comparable to that observed. The same model is also able to reproduce the observed values or limits on N(H I), N(Mg II), N(Si II), and N(S II). A careful study of the ionization properties in this gas will require information on a range of species with differing ionization behavior.

In our analysis of the Mg II, Si II, and S II absorption relative to H I we have assumed that the ultraviolet absorption line data and the H I emission-line data are directly comparable. However, the difference in sampling (infinitesimal solid angle for the ultraviolet absorption measurements vs. 20′ beam for the H I radio data) may be affecting our analysis. Radio measurements at higher angular resolution for the direction to H1821+643 would be valuable.

We have also ignored the possible consequences of the presence of interstellar dust at large Galactocentric distances. If dust is present, then the intrinsic abundances of Mg and Si may be larger than those derived above for the gas phase.

5. HIGHLY IONIZED GALACTIC GAS

The strong C IV $\lambda\lambda$1548, 1550 absorption doublet illustrated in Figure 2 reveals a complex profile spanning the LSR velocity range from about +40 to −150 km s^{-1} with the possible detection of a weak additional component at −213 km s^{-1}. The N V $\lambda\lambda$1238, 1242 absorption, while strong, extends over a narrower velocity range from approximately +40 to −60 km s^{-1}. Each of the four absorption components listed in Table 3 are discussed in the following sections.

5.1. C IV *and* N V *Absorption at* −8 km s^{-1}

The strongest portion of the C IV absorption profile can be fitted with a Gaussian absorption component (component 1 in Table 3) with $v_{LSR} = -8.2 \pm 3.7$ km s^{-1}, $b = 28.4 \pm 3.3$ km s^{-1}, and N(C IV) = $(10.4 \pm 1.4) \times 10^{13}$ cm^{-2}. This portion of the C IV absorption appears to trace the gas responsible for component 1 seen in the N V doublet with $v_{LSR} = -6.9 \pm 5.7$ km s^{-1}, $b = 34.8 \pm 4.4$ km s^{-1}, and N(N V) = $(14.3 \pm 2.6) \times 10^{13}$ cm^{-2}. The large line widths and the small ratio of C IV to N V ($\sim$0.73) imply the absorbing gas is hot. If the line widths are entirely produced by thermal Doppler broadening the implied gas temperatures are $(5.8 \pm 1.4) \times 10^5$ K for the C IV line and $(1.0 \pm 0.3) \times 10^6$ K for the N V line. Allowing for turbulence or blending of unresolved components would reduce the temperatures. The observed C IV to N V column density ratio occurs for gas in collisional ionization equilibrium with a solar C to N abundance ratio if the gas temperature is $\sim 1.7 \times 10^5$ or $(\sim 6\text{–}10) \times 10^5$ K (Sutherland & Dopita 1993).

The low velocity of component 1 suggests the site of the absorbing gas is relatively close to the Sun (i.e., $d <$ several kpc). Much of the gas seen in component 1 may be associated with Galactic radio loop III since the sight line passes close to the outer boundary of this radio loop (see § 3). If these Galactic radio loops define the sites of old supernova explosions, the cooling of hot gas associated with those events may explain much of the absorption. The association of highly ionized interstellar gas and Galactic radio loops has also been proposed for the sight line to 3C 273 (Burks et al. 1991; Savage et al. 1993a) which passes through the edge of radio loop I.

The gas seen in component 1 resembles the higher temperature gas of the two gas types found by Savage, Sembach, & Cardelli (1994) toward the inner Galaxy star HD 167756 at 4 kpc in the direction $l = 351\overset{\circ}{.}5$ and $b = -12\overset{\circ}{.}3$. That gas was characterized by N(C IV)/N(N V) $\sim$ 1.0, b(C IV) $\sim$ 27 km s^{-1}, and b(N V) $\sim$ 33 km s^{-1} and $T > 2 \times 10^5$ K. Such regions of interstellar absorption appear to provide substantial contributions to interstellar C IV and N V absorption. The gas found in component 1 toward H1821+643 provides support for the idea that some of the high-ionization absorption found in the interstellar gas is associated with absorption produced in cooling supernova bubbles (Slavin & Cox 1992, 1993). The observed column density ratio, N(C IV)/N(N V) $\sim$ 0.7, is similar to that expected for the nonequilibrium cooling of hot gas with solar abundances at constant pressure [N(C IV)/N(N V) $\sim$ 0.8; Edgar & Chevalier 1986]. The existence of such regions may help to explain the high degree of inhomogeneity of the hot interstellar gas as revealed in the absorption lines of C IV, N V, and O VI (Sembach & Savage 1992; Shelton & Cox 1994).

5.2. C IV *Absorption at* −70 km s^{-1}

The C IV absorption component 2 with $\langle v_{LSR} \rangle = -70 \pm 3.7$ km s^{-1}, $b = 18.0 \pm 4.1$ km s^{-1} and N(C IV) = $(6.0 \pm 1.6) \times 10^{13}$ cm^{-2} has N(N V) $< 3.5 \times 10^{13}$ cm^{-2} (3 σ). Thus N(C IV)/N(N V) > 1.7 in this component, which implies that the gas has very different properties than the gas associated with component 1. The value of b(C IV) = 18.0 km s^{-1} constrains the temperature of the gas in component 2 to $T < 2.3 \times 10^5$ K.

Component 2 appears to be kinematically associated with gas above the Perseus spiral arm which has $v_{LSR} \approx -70$ to −80 km s^{-1} in the direction $l = 94°$, $b = 0°$ (Kepner 1970). The H1821+643 sight line passes $\sim$1.5 kpc over the arm. Kepner (1970) was able to trace H I emission associated with the Perseus spiral arm to $z \sim +1.5$ kpc. Similarly, Reynolds (1986) has found Hα emission from photoionized gas above the Perseus arm to $z \sim 1$ kpc.

An enhancement in the amount of C IV over the Perseus spiral arm supports the idea that highly ionized gas in the halo can originate from the energetic activity occurring in OB associations. The liberation of the hot gas into the halo by either fountain flows (Shapiro & Field 1976; Bregman 1980; Shapiro & Benjamin 1991) or by chimney flows (Bruhweiler et al. 1980; McCray & Kafatos 1987; Norman & Ikeuchi 1989) is expected to be linked to the OB associations found in the spiral arms.

Since we do not detect N V in component 2 with N(C IV)/N(N V) > 1.7, the gas is clearly cooler than the gas of component 1 where N(C IV)/N(N V) ≈ 0.7. The component 2 gas may represent the second type of highly ionized gas found by Savage et al. (1994) in which N(C IV)/N(Si IV) ≈ 3.0 and N(C IV)/N(N V) > 6.0. However, it will be necessary to obtain measures of Si IV in component 2 to firmly establish this connection.

5.3. C IV *Absorption at* −120 km s^{-1}

The C IV absorption in component 3 with $\langle v_{LSR} \rangle = -120.3 \pm 5.4$ km s^{-1}, $b = 24.8 \pm 3.1$ km s^{-1}, and N(C IV) = $(6.1 \pm 1.1) \times 10^{13}$ cm^{-2} has N(N V) $< 4.2 \times 10^{13}$ cm^{-2} (3 σ). Thus, N(C IV)/N(N V) > 1.5 in this component, which implies that this gas also has different properties than the gas associated with component 1.

The high velocity of component 3 possibly associates the gas with the outer arm and distant warp of the Milky Way. The kinematically implied Galactocentric distance from the rotation curve shown in Figure 2 is $\sim$24 kpc, and the distance away from the Galactic midplane is $z \sim 7$ kpc. Recent H I studies of the distant warp of the Milky Way in this direction have traced neutral gas to $z \sim +8$ to 10 kpc at $R_G \sim 24$ kpc (Diplas & Savage 1991). The C IV we are seeing at high velocity may arise in hot collisionally ionized gas. The width of the observed line ($b = 24.8$ km s^{-1}) constrains the temperature to $T < 4.4 \times 10^5$ K. Such hot gas might arise in the interface between a much hotter exterior medium and the warm gas providing the Mg II and Si II absorption. Perhaps the C IV absorption is associated with the type of turbulent mixing layer first discussed by Begelman & Fabian (1990). In fact, these authors suggested that the hot gas layers might occur in the outer parts of galaxies due to the relative motion of the warm neutral outer Galaxy gas and a hotter exterior medium, for which unfortunately, there are very few observational constraints (see Fabian 1991).

We have not mentioned a Galactic fountain (Shapiro & Field 1976; Bregman 1980) in this discussion because the warped outer gaseous layer of the Galaxy extends well beyond the stellar disk (Diplas & Savage 1991). Therefore, the collective explosive events that are required to drive a Galactic foun-

tain (multiple supernova explosions in OB associations) are unlikely to occur in this region of the Milky Way.

The C IV absorption could also occur in warm ($T \sim 10^4$ K) gas photoionized by the extragalactic EUV radiation field. To test this possibility, we have computed ionic column densities for the outer Galaxy using the photoionization code CLOUDY (Ferland 1991). We model the warp as an infinite slab of constant density illuminated on one side. We adopt the model AGN spectrum of Madau (1992), where the energy distribution is a broken power-law form with index $= -0.7$ at wavelengths shorter than Lyα, and index $= -1.5$ at wavelengths longer than Lyα. The opacity of intervening absorbing clouds is ignored. With this model, the only parameter needed to fix the ionizing radiation field is the mean intensity at the Lyman limit frequency, J_ν(LL). Various studies (Bochkarev & Sunyaev 1977; Kutyrev & Reynolds 1989; Songaila, Bryant, & Cowie 1989; Miralda-Escude & Ostriker 1990; Stocke et al. 1991; Madau 1992; Maloney 1993; Corbelli & Salpeter 1993) constrain the value of J_ν(LL) locally to the range 6×10^{-24} to 2×10^{-22} ergs s^{-1} Hz^{-1} cm^{-2} sr^{-1}.

Figure 4 shows the results of the calculations with J_ν(LL) = 10^{-22} ergs s^{-1} Hz^{-1} cm^{-2} sr^{-1} and 10% solar abundances. The assumed abundances are selected to be less than solar to allow for a Galactocentric abundance gradient. The column densities of Si II, Mg II, S II, Si IV, C IV, and N V are shown in Figure 4 as functions of the logarithm of the ionization parameter, Γ, which is the ratio of ionizing photon density to gas density. The corresponding total gas density for the adopted J_ν(LL) is shown on the top of the figure. The ionic column densities roughly scale linearly with the metallicity of the gas. The column densities in the slab were calculated by integrating along a sight line perpendicular to the slab until log N(H I) = 18.79, the value observed over the velocity range from -100 to -150 km s^{-1}. Near log $\Gamma = -3.1$ which corresponds to a total gas density log $n_{tot} = -2.25$, the model yields column densities for C IV, Si II, Mg II, and S II of 6.5×10^{13}, 1.4×10^{14}, 1.3×10^{14}, and 5.6×10^{13} cm^{-2}, respectively. These numbers are consistent with the observed column densities in the -120 km s^{-1} component. With log $n_{tot} = -2.25$ or 5.6×10^{-3} cm^{-3}, the layer thickness is 6.2 kpc and the neutral hydrogen fraction, H I/H$_{tot}$ = 0.056. Photoionization in the low-density gas of the outer Galaxy is a plausible explanation for the origin of C IV at -120 km s^{-1}.

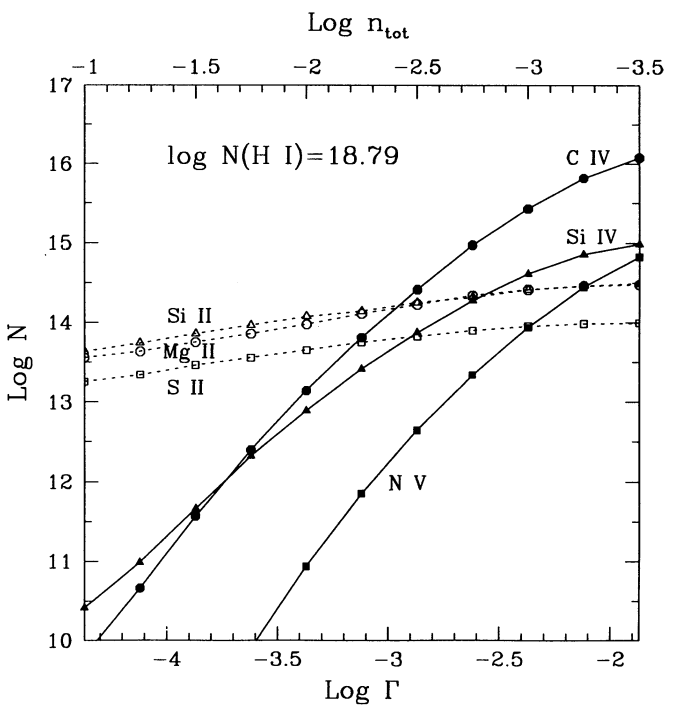

FIG. 4.—Results of a simple plane parallel photoionization model for the outer Galaxy illuminated by the EUV extragalactic background radiation field. The curves plotted are logarithmic column densities for Si II, Mg II, S II, C IV, Si IV, and N V vs. the logarithm of the ionization parameter, log Γ. The top scale shows the corresponding total (neutral + ionized) hydrogen density. The ionizing radiation spectrum at the Lyman limit is assumed to have a mean intensity of J_ν(LL) = 10^{-22} ergs^{-1} Hz^{-1} cm^{-2} sr^{-1} and the metallicity is assumed to be 1/10 solar. The column densities apply to gas in the outer Galaxy into the region where log N(H I) = 18.79, which corresponds to the observed value of the H I column density associated with the -120 km s^{-1} absorption. For log $\Gamma = -3.1$ which corresponds to log $n_{tot} = -2.25$, the model yields values of N(C IV), N(Si II), N(Mg II), and N(S II) consistent with the observations.

5.4. *Possible* C IV *Absorption at* -213 km s^{-1}

The weak absorption component 4 which we attribute to C IV at $\langle v_{LSR} \rangle = -213.3 \pm 3.0$ km s^{-1} with $b = 11.6 \pm 2.7$ km s^{-1} and N(C IV) = $(1.2 \pm 0.3) \times 10^{13}$ cm^{-2} is a 4 σ detection in the C IV λ1548 line. A corresponding absorption in the C IV λ1550 line (see Fig. 2) only has a 2 σ level of significance, which is consistent with the factor of 2 difference in f-value. The value of b(C IV) for the absorption implies $T < 1 \times 10^5$ K. While we believe the correct identification for this feature is C IV, we cannot rule out the possibility of a contaminating Lyα line at redshift 0.27257. The velocity of this absorption is interesting because it is similar to the expected limiting velocity for distant Milky Way gas of $\sim -190 \pm 20$ km s^{-1} for the direction to H1821+643 (see rotation curve in Fig. 2). A feature near -213 km s^{-1} is not detected in any of the other species we have observed including H I, S II, Mg II, and Si II.

The absorption may represent the detection of a new type of Milky Way high-velocity cloud, a cloud only seen in the high-ionization species. A highly ionized high-velocity cloud (also only seen in C IV) has been detected toward Markarian 509 by Sembach et al. (1995b). In that case, very strong C IV absorption extends from -180 to -340 km s^{-1} and is clearly recorded in both components of the C IV doublet.

6. INTERGALACTIC ABSORPTION LINES

The observed absorption lines we identify as intergalactic are listed in Table 3. Lines that cannot be identified with known redshift systems (either metal-line systems or Lyα systems) are assumed to be intergalactic Lyα lines.

We detect the Lyγ and the C III 977.020 absorption associated with the $z = 0.2967$ redshift system. This system has a nearly identical redshift as the quasar H1821+643 itself ($z_{em} = 0.2966$; see Bahcall et al. 1992) and shows moderately to highly ionized species such as C III, Si IV, C IV, and O VI, in addition to Lyα and Lyβ. This system belongs to the category of "associated absorption systems," which are almost certainly intrinsic to the quasars themselves (either the region surrounding the nucleus or the host galaxy).

We also detect the Lyβ line at the redshift $z = 0.22489$ whose Lyα line was detected in the FOS spectrum of H1821+643 (Bahcall et al. 1992, 1993). As noted by Bahcall et al. (1992), this Lyα system has a redshift that is nearly identical to that of a foreground galaxy (galaxy G at $z = 0.2265$, see Schneider et al. 1992) in the field of the quasar. The galaxy (G) has a projected

distance of 90 kpc from the quasar line of sight. It is likely that the Lyα and Lyβ absorption arise either from the extended disk/halo of galaxy G or from the intracluster gas (if galaxy G resides in a cluster). This is perhaps not too surprising, given the recent study of Lanzetta et al. (1995) who concluded that 35%–65% of Lyα systems at $z < 1$ may be associated with luminous galaxies. If indeed the $z = 0.22489$ Lyα system arises from extended disk or halo gas surrounding galaxy G or from the intracluster gas, one might expect to see metal absorption originating from the same gas. Our spectrum shown in Figure 1 covers the Si II 1260.422 line (observed wavelength 1543.88 Å), and the O VI 1031.926 line (observed wavelength 1264.00 Å). The Si II absorption is not detected, with a 3 σ upper limit on the Si II column density of $N(\text{Si II}) < 2.7 \times 10^{12}$ cm^{-2}. The O VI 1031.926 absorption, if present, is blended with a Lyα line at 1264.138 Å. The shape of the 1264.138 Å line (broad with a relatively flat peak absorption) is suggestive of blending of two lines. Unfortunately the O VI 1037.617 line, which is expected to be at 1270.97 Å, is beyond our spectral coverage, so no independent check is possible. The existing FOS spectrum of Bahcall et al. (1992, 1993) covers many lines in this system but is not sensitive enough to put any useful constraints on other metal ion column densities. A detailed study of the galaxies in the quasar field and a sensitive measurement of the metallicity in this system is highly desirable.

Our Lyα line list is estimated to be complete to a rest-frame equivalent width level of $\approx$60 mÅ, which is similar to the $\approx$50 mÅ completeness limit for the GHRS observations of the quasar 3C 373 (Morris et al. 1991; Weymann 1991). This allows for a meaningful comparison of the Lyα line density along the two different sight lines. These two sight lines are the only published ones with such high detection sensitivity. Note that Bruhweiler et al. (1993) have already found that the sight lines to 3C 273 and PKS 2155−304 have similar Lyα line densities for stronger lines with $W_\lambda(\text{rest}) > 160$ mÅ. Along the path to H1821+643, we detect five Lyα lines with $W_\lambda(\text{rest}) > 60$ mÅ over a total redshift path of 0.057. This implies a Lyα cloud density per unit redshift of $dN/dz = 88 \pm 39$. For 3C 273, nine lines with $W_\lambda(\text{rest}) > 60$ mÅ are detected over a redshift path of 0.135, or $dN/dz = 67 \pm 22$. The similar values of dN/dz are consistent with the interpretation that the Lyα systems are cosmological entities rather than intrinsic to the quasars themselves. Combining the two sight lines, we obtain a low-redshift cloud density $dN/dz = 73 \pm 19$ for Lyα lines with rest-frame equivalent width greater than 60 mÅ.

Similarly, we can compare the intrinsic cloud parameters (Doppler parameter and H I column density) for the H1821+643 and 3C 273 sight lines. We find a mean Doppler parameter $\langle b \rangle = 37 \pm 11$ km s^{-1} for the six Lyα clouds along the path to H1821+643 and $\langle b \rangle = 40 \pm 25$ km s^{-1} for the 14 Lyα clouds for the 3C 273 line of sight. These means are consistent with each other and are similar to the means for Lyα clouds detected in the optical window at $z > 1.7$, where $\langle b \rangle = 35 \pm 16$ km s^{-1} (see Carswell 1988 and references therein). For the combined GHRS sample, $\langle b \rangle = 39 \pm 21$ km s^{-1}. The N(H I) of the clouds ($\sim 10^{13}$ to a few times 10^{14} cm^{-2}) along the two sight lines are also similar. The lack of the very high column density clouds in the GHRS sample is probably the result of the small sample size. Given the small sample size of the low-z Lyα clouds, a detailed comparison of the cloud parameters at low-z and high-z is not justified at this point. However, the limited available data suggest no obvious evolution in the Doppler parameter between $z = 2$ and 0. The strong evolution in dN/dz has been the topic of many studies (see Bahcall et al. 1993 and references therein).

7. SUMMARY

We present intermediate resolution (FWHM $\sim$ 10–20 km s^{-1}) GHRS ultraviolet observations of interstellar and intergalactic absorption lines in the spectrum of the bright quasar H1821+643.

1. The interstellar features detected include lines of S II, Si II, Mg II, C IV, and N V. The intergalactic lines detected include Lyα (six lines), Lyβ (two lines), Lyγ, and C III.

2. Over the velocity range from -100 to -150 km s^{-1}, which probably traces absorption in the outer Milky Way with $R_G > \sim 20$ kpc, we estimate Si II/H I, Mg II/H I, and S II/H I are 0.92 ± 0.20, ≥ 0.25, and ≤ 1.5 times the abundances of these elements found in the Sun. Including a large correction for the likely effects of ionization suggests the intrinsic abundances in this gas are very roughly 1/10 solar.

3. A strong C IV and N V absorption component centered near $v_{\text{LSR}} = -8$ km s^{-1} has $N(\text{C IV})/N(\text{N V}) = 0.7$. This gas is probably hot ($T > 2 \times 10^5$ K) and may be associated with the energetic events responsible for Galactic radio loop III.

4. An intermediate-velocity C IV absorption component at -70 km s^{-1} is probably associated with highly ionized gas situated ~ 1.5 kpc above the Perseus spiral arm. The gas could be collisionally ionized and hot with $T < 2 \times 10^5$ K (as inferred from $b = 18$ km s^{-1}) or photoionized and warm.

5. High-velocity C IV absorption at -120 km s^{-1} may arise in highly ionized gas above the outer spiral arm of the Milky Way. Assuming corotation of disk and halo gas, a velocity of -120 km s^{-1} occurs at a Galactocentric distance of ~ 24 kpc and a distance away from the Galactic plane of $z \sim 7$ kpc. A simple photoionization model reveals that a plausible explanation for the ionization is photoionization by the extragalactic EUV background in the low-density gas of the outer Milky Way.

6. We observe five low-redshift Lyα lines with $W_\lambda(\text{rest}) > 60$ mÅ over a redshift path of 0.057. The H1821+643 and 3C 273 sight lines exhibit a similar number density of low-redshift Lyα lines. Combining the results for the two sight lines, we obtain a Lyα cloud density $dN/dz = 73 \pm 19$ for $0 < z < 0.3$ with $W_\lambda(\text{rest}) > 60$ mÅ.

The observations presented here would not have been possible without the dedicated efforts of many people associated with the *HST* and GHRS projects. Helpful comments about the manuscript from Todd Tripp and the referee are appreciated. We thank Jennifer Sandoval for her assisting with the data handling. Support for this work was provided by NASA through grant numbers GO-5299.01-93A and HF-1038.01-92A (for K. R. S.) from the Space Telescope Science Institute, which is operated by the Association of Universities for Research in Astronomy, Inc. for NASA under contract NAS 5-26555.

REFERENCES

Acker, A., Marcout, J., Ochsenbien, F., Stenholm, B., Tyenda, R., & Marcout, J. 1992, Strasbourg-ESO Catalogue of Galactic Planetary Nebulae, Vol. 2 (Garching: ESO), 334
Anders, E., & Grevesse, N. 1989, Geochim. Cosmochim. Acta, 53, 197
Bahcall, J. N., et al. 1993, ApJS, 87, 1
Bahcall, J. N., Jannuzi, B. T., Schneider, D. P., Hartig, G. F., & Green, R. 1992, ApJ, 397, 68
Begelman, M. C., & Fabian, A. C. 1990, MNRAS, 244, 26P

Berkhuijsen, E., Haslam, C. G. T., & Salter, C. J. 1971, A&A, 14, 252
Bochkarev, N. G., & Sunyaev, R. A. 1977, Sov. Astron., 21, 542
Brandt, J., Heap, S. R., Beaver, E. A., Boggess, A., Carpenter, K. G., et al. 1994, PASP, 106, 890
Bregman, J. N. 1980, ApJ, 236, 577
Bruhweiler, F. C., Boggess, A., Norman, D. J., Grady, C. A., Urry, C. M., & Kondo, J. 1993, ApJ, 409, 199
Bruhweiler, F. C., Gull, T. R., Kafatos, M., & Sofia, S. 1980, ApJ, 238, L27
Burks, G. S., York, D. G., Blades, J. C., Bohlin, R. C., & Wamsteker, W. W. 1991, ApJ, 381, 55
Burton, W. B. 1988, in Galactic and Extragalactic Radio Astronomy, ed. K. Kellermann & G. L. Verschuur (New York: Springer), 295
Burton, W. B., & te Lintel Hekkert, P. 1985, A&AS, 65, 427
Carswell, R. F. 1988, in QSO Absorption Lines: Probing the Universe, ed. J. C. Blades, D. A. Turnshek, & C. A. Norman (Cambridge: Cambridge Univ. Press), 91
Corbelli, E., & Salpeter, E. E. 1993, ApJ, 419, 104
Danly, L. 1989, ApJ, 342, 785
de Boer, K. S., Altan, A. Z., Bomans, D. J., Lilienthal, D., Mochler, S., van Woerden, H., Wakker, B. P., & Bregman, J. N. 1994, A&A, 286, 925
Diplas, A., & Savage, B. D. 1991, ApJ, 377, 126
Dupree, A. K., & Raymond, J. C. 1983, ApJ, 275, L71
Edgar, R. J., & Chevalier, R. A. 1986, ApJ, 310, L27
Edgar, R. J., & Savage, B. D. 1992, ApJ, 396, 124
Fabian, A. C. 1991, in IAU Symp. 144, The Interstellar Disk-Halo Connection in Galaxies, ed. H. Bloemen (Dordrecht: Kluwer), 237
Ferland, G. J. 1991, Ohio State Internal Report 91-01
Grauer, A. D., & Bond, H. E. 1984, ApJ, 277, 211
Haud, U. 1988, A&A, 198, 125
Heiles, C. 1984, ApJS, 55, 485
Kepner, M. 1970, A&A, 5, 444
Kirhakos, S., Sargent, W. L. W., Schneider, D. P., Bahcall, J. N., Jannuzi, B. T., Mauz, D., & Small, T. A. 1994, PASP, 106, 646
Kohoutek, L. 1963, Bull. Astron. Inst. Czechoslovakia, 14, 70
Kuntz, K., & Danly, L. 1992, PASP, 104, 1256
Kutyrev, A. S., & Reynolds, R. J. 1989, ApJ, 344, L9
Lanzetta, K. M., Bowen, D. V., Tytler, D., & Webb, J. K. 1995, ApJ, 442, 538
Lockman, F. J., & Savage, B. D. 1995, ApJS, 97, 1
Lu, L., Savage, B. D., & Sembach, K. R. 1994, ApJ, 426, 563
Madau, P. 1992, ApJ, 389, L1
Maloney, P. 1993, ApJ, 414, 41
McCray, R., & Kafatos, M. 1987, ApJ, 317, 190
Miralda-Escude, J., & Ostriker, J. P. 1990, ApJ, 350, 1
Morris, S. L., Weyman, R. J., Savage, B. D., & Gulliland, R. L. 1991, ApJ, 377, L21
Morton, D. C. 1991, ApJS, 77, 119
Norman, C. A., & Ikeuchi, S. 1989, ApJ, 345, 372
Reynolds, R. 1986, in Proc. NRAO Conference on Gaseous Galactic Halos, ed. J. N. Bregman & F. J. Lockman (Greenbank: NRAO), 53
Savage, B. D., Lu, L., Bahcall, J. N., Bergeron, J., Boksenberg, A., et al. 1993a, ApJ, 413, 116
Savage, B. D., Lu, L., Weymann, R., Morris, S., & Gulliland, R. 1993b, ApJ, 404, 124
Savage, B. D., & Sembach, K. R. 1991, ApJ, 379, 245
Savage, B. D., Sembach, K. R., & Cardelli, J. A. 1994, ApJ, 420, 183
Schneider, D. P., Bahcall, J. N., Gunn, J. E., & Dressler, A. 1992, AJ, 103, 1047
Sembach, K. R., Danks, A., & Savage, B. D. 1993, A&AS, 100, 107
Sembach, K. R., & Savage, B. D. 1992, ApJS, 83, 147
Sembach, K. R., Savage, B. D., & Lu, L. 1995a, ApJ, 439, 672
Sembach, K. R., Savage, B. D., Lu, L., & Murphy, E. 1995b, ApJ, in press
Shapiro, P. R., & Benjamin, R. 1991, PASP, 103, 923
Shapiro, P. R., & Field, G. B. 1976, ApJ, 205, 762
Shaver, P. A., McGee, R. X., Newton, L. M., Danks, A. C., & Pottasch, S. R. 1983, MNRAS, 204, 53
Shelton, R., & Cox, D. P. 1994, ApJ, 434, 599
Slavin, J. D., & Cox, D. P. 1992, ApJ, 392, 131
———. 1993, ApJ, 417, 187
Soderblom, D. R., Hulbert, S. J., Leither, C., & Sherbert, L. E. 1994, Goddard High Resolution Spectrograph Instrument Handbook, Version 5 (Baltimore: Space Telescope Science Institute)
Songaila, A., Bryant, W., & Cowie, L. L. 1989, ApJ, 345, L71
Spitzer, L., & Fitzpatrick, E. 1993, ApJ, 409, 299
Spoelstra, T. A. Th. 1972, A&A, 21, 61
Stocke, J. T., Case, J., Donahue, M., Shull, J. M., & Snow, T. P. 1991, ApJ, 374, 72
Sutherland, R. S., & Dopita, M. A. 1993, ApJS, 88, 253
Vallerga, J. V., Vedder, P. W., Craig, N., & Welsh, B. Y. 1993, ApJ, 411, 729
Verschuur, G. L. 1993, ApJ, 409, 205
Wakker, B. P., & van Woerden, H. 1991, A&A, 250, 509
Weymann, R. J. 1991, in The First Year of *HST* Observations, ed. A. L. Kinney & J. C. Blades (Baltimore: Space Telescope Science Institute), 58